Hindawi
Advances in Civil Engineering
Volume 2018, Article ID 4735423, 16 pages
https://doi.org/10.1155/2018/4735423

Research Article

Axial Uplift Behaviour of Belled Piers in Coarse-Grained Saline Soils

Jian Xu,[1] Jianwei Ren,[1] Songhe Wang,[2] Long Jin,[3] and Jun Yuan[4]

[1]*School of Civil Engineering, Xi'an University of Architecture and Technology, Xi'an, Shaanxi 710055, China*
[2]*Institute of Geotechnical Engineering, Xi'an University of Technology, Xi'an, Shaanxi 710048, China*
[3]*State Key Laboratory of Road Engineering Safety and Health in Cold and High-altitude Region, CCCC First Highway Consultants Co., Ltd., Xi'an, Shaanxi 710075, China*
[4]*Northwest Electric Power Design Institute Co., Ltd. of China Power Engineering Consulting Group, Xi'an, Shaanxi 710075, China*

Correspondence should be addressed to Songhe Wang; wangsonghe@126.com

Received 30 July 2018; Accepted 30 September 2018; Published 4 November 2018

Academic Editor: Eric Lui

Bearing capacity of belled pier foundation is critical in designing transmission lines in coarse saline soil region. This paper describes model test results on belled pier foundations. Axial uplift behaviours including failure modes, load-displacement curves, and ultimate uplift bearing capacity were discussed. The failure planes in four cases were obtained from pulled out cone-shaped bodies. An empirical equation was developed with a critical parameter of an uplift angle in design. Results indicate the range where the ground uplift shows circular extension at higher loads and the overall shear failure finally occurred. The load-displacement curves are primarily softening, and the uplift bearing capacity for coarse-grained saline soils (CSS) in the crystalline state increases at larger thickness, higher than that in dissolved state. Failure planes all exhibit approximately linear change from bottom to up. The angles of uplift for soils in crystalline and dissolved states can be taken as 34° and 18°, while 32° for the conventional for the sake of safety. Uplift behaviour of belled piers in CSS was modelled incorporating a practical interface model, with both failure planes and plastic range.

1. Introduction

Massive infrastructures have been designed and constructed in Northern China, such as the West-East electricity transmission project, and have to face the problematic soils, e.g., coarse-grained saline soils, especially those distributed in the Gobi Desert or the desert margin in inland areas [1, 2]. The coarse-grained saline soils experienced cyclic salification and desalination due to complex processes that salt in soils periodically exists in crystalline or dissolved state, accompanied by a continuing migration and accumulation of dissolved salt, resulting in particular engineering properties [3, 4]. Experiments prove that this kind of problematic soils exhibits particular behaviours because of that better bearing capacity can be obtained as soils crystallized with good bonding between particles. However, for these soils, dissolved salt may induce wetting collapse in ground, leading to damages in infrastructures [5, 6]. This kind of behaviours differs from both cohesive soils with good bonding between particles and coarse soils with better drainage [7–10]. Thus, the design of foundations involving the coarse-grained saline soil deserves urgent attentions for its bearing characteristics and ground treatment scheme.

The engineering design for the foundations in coarse-grained saline soils lacks a reasonable consideration of the mechanism and characteristic value for bearing capacity, selection of foundation type, and the construction method. For design tasks when such particular geological conditions are involved, the designers often follow the principles that are applicable for conventional soils and conservative plans for design. More importantly, the bearing capacity for this particular material cannot be fully utilized, especially for cases when soils maintain a crystalline state. So far, the belled pier foundation is

frequently used in designing a transmission line. This kind of foundation well utilizes the bearing capacity of soils and also has the merit that no redundant abandoned soils and water will be produced during construction [11, 12].

The other aspect involved in uplift behaviour of belled pier is the failure mode in foundations. Ikeda et al. [13] conducted numerical analysis of the uplift problems to assess the progressive and localized failure in foundations based on an elastoplastic finite element method, which was verified by centrifugal experiments. The uplift bearing capacity and the load-displacement relationship have been investigated by the scholars [14–16]; however, little work has been done on the uplift capacity of the belled pier constructed in coarse-grained saline soils.

Considering the urgent needs of transmission line construction, four groups of model tests were carried out on the belled pier foundations constructed on two-layered soils, coarse-grained saline soil layer above, and conventional coarse soils (CS) layer. Two occurrence modes and three different thicknesses for saline soils were considered. The uplift behaviours of the belled pier foundations including the apparent failure mode, ground displacement, load-displacement curves, and ultimate uplift bearing capacity were measured, aiming to provide guidance for the foundation design in coarse-grained saline soils.

2. Test Plan

2.1. Brief Introduction to the Coarse-Grained Saline Soils. Most of the saline soils are distributed in areas where the climate is arid or semiarid except for the coastal regions in China, with less precipitation but larger evaporation. Affected by the climate, the occurrence of salt in saline soils shows seasonal variations that soils tend to desalinate in summer due to intensive and larger rainfall, while in both spring and autumn, evaporation exceeds the precipitation and thus the salt accumulated in ground surface cannot be leached, inducing a further salification in soils [17, 18]. The topographic features for saline soils developed are mainly lowland, inland basin, and marsh land, e.g., the Hexi Corridor, inland basin, and the Gobi Desert in Xinjiang Province, China. The salt was migrated from high to low areas with surface and underground runoff and subsequently accumulated in lower land. In addition, the coupling of leaching and evaporation due to both precipitation and runoff generally led to the layered or nest-shaped gathering of salt and both the crystalline salt bed and saline lens with thickness of a few centimetres can be easily observed in saline soil regions, called surface aggregation. The sampling site, i.e., the Multicolored Bay, located in the north of Jimsar County in Xinjiang Province, is a scenic area with coarse-grained saline soils widely distributed. Figure 1 presents the strata feature for coarse-grained saline soils in this area. Figure 2 illustrates the variation of dissolved salt with depth for three test sites in the Multicolored Bay. The dissolved salt is primarily distributed within the depth of 3.0 m and dissolved salt significantly decreases with depth. Saline soils show discontinuity and inhomogeneity in horizontal directions and most of the dissolved salt gathered along the principal line of torrent in gullies.

2.2. Specimen Preparation. The coarse-grained saline soil samples were taken from three test sites in the Multicolored Bay of Xinjiang Province. The water content of soils is about 4%, and the dry density is within the range of 2.15–2.26 g/cm^3. The coarse-grained saline soils are constituted by three kinds of soils, i.e., gravel, medium sand, and silty loess, with the mass percentages of 55%, 20%, and 25%, respectively. The grain sizes for gravel and medium sand are 2–20 mm and 0.2–2 mm, respectively, while for silty loess the particles with a size smaller than 2 mm take a dominant proportion. The salinity tests for soils from their three sites, five kinds of common ions measured, are conducted as shown in Figure 3. It clearly shows that the soils' sulphate ion accounts for a major proportion of the total dissolved salt content, followed by the calcium and chloride ions, while the contents for both bicarbonate ion and magnesium ion are lower. For the model tests, coarse-grained saline soils were produced by the above three soils and the mass percentage is identical to that in three sites to keep consistency in the composition of particles. Besides, the easily obtained anhydrous sodium sulphate is used in model tests, with the mass percentage of 8%. The coarse-grained saline soil samples were prepared by mixing the three soils that were calculated and weighted according to the proportions abovementioned. The soil samples were placed in plastic bags for 24 h to ensure the uniformity of moisture. The prepared soil samples basically consist of six different grain sizes, i.e., 20–60 mm (12.13%), 5–20 mm (44.25%), 2–5 mm (8.03%), 0.5–2 mm (19.04%), 0.25–0.5 mm (7.14%), and <0.25 mm (9.41%).

2.3. Test Procedure. By referencing the detailed design of the South Hami-Zhengzhou transmission line, the test pit and belled pier foundations were designed with a scaling factor of 10%. The dimensions of the test foundation pit were 2.8 m × 2.8 m × 1.5 m, and the load-bearing brick column was heightened to 2.2 m. The fired common bricks of size (240 mm × 115 mm × 53 mm) were used, with cement mortar filled between bricks. The standard compressive strength of both bricks and cement mortar are 15.0 and 5.0 MPa, respectively. The specific sizes of the belled piers are presented in Figures 4(a) and 4(b). The ratio of depth to diameter, i.e., $(H-n)/D$, is 2.5, in which, H is the embedded depth of foundations, n is the height of the expanded column, and D is the diameter of the bottom plate. The thickness for CSS, h, is used as a controlling variable to evaluate the uplift bearing capacity of belled pier foundation. Four groups of experiments were carried out in the laboratory, corresponding to four working conditions. The CSS in the crystalline state were utilized in the first three groups, with the thicknesses of 50, 100, and 150 mm, identified as Test I, Test II, and Test III, respectively. While for the fourth group, 100 mm thick coarse saline soils in the dissolved state were used, identified as Test IV. The sodium sulphate solutions with a mass percentage of 8.0% were sprayed on

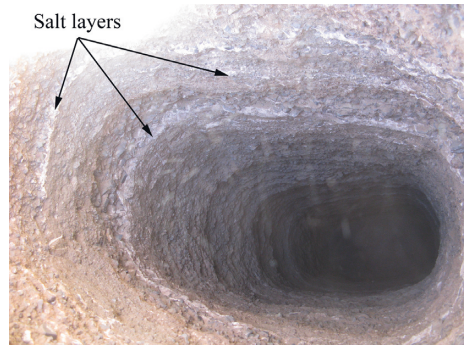

Figure 1: Strata feature for coarse-grained saline soils.

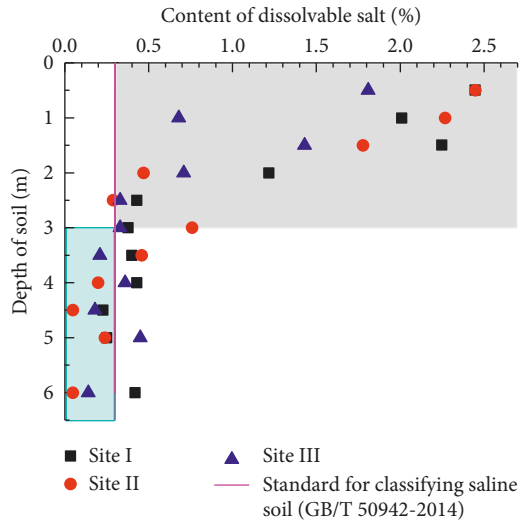

Figure 2: Variation of dissolved salt content with depth.

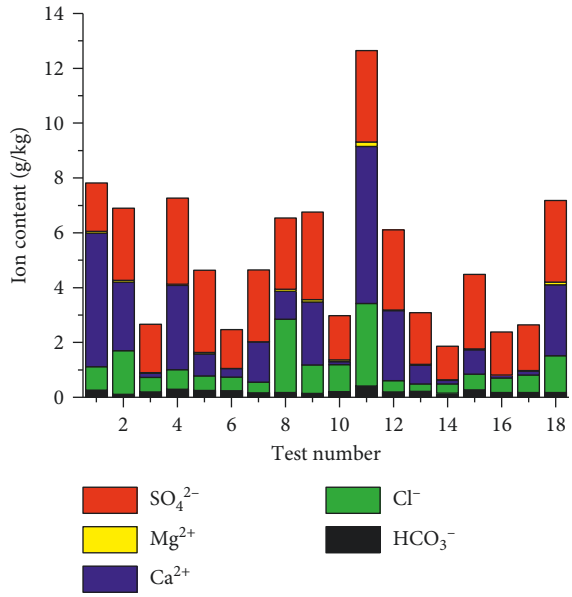

Figure 3: Salinity determination for coarse-grained saline soils.

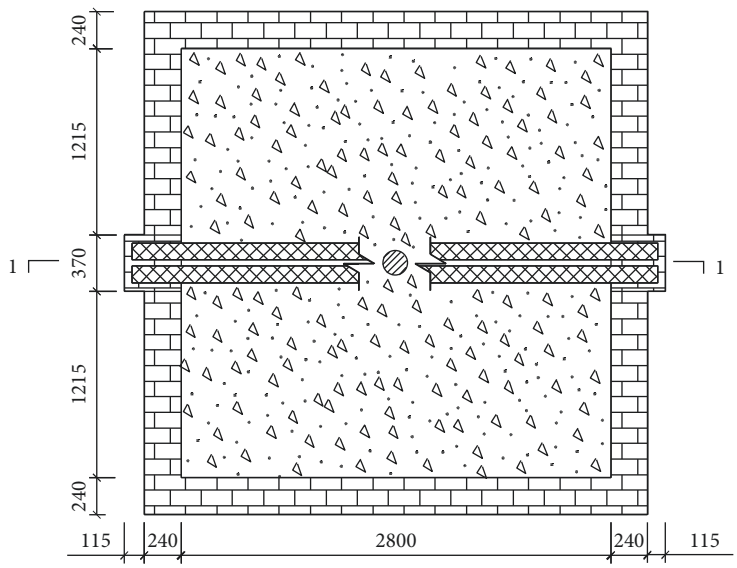

Unit: mm

Brick masonry

Steel beam

Belled pier foundation

Coarse-grained saline soil

(a)

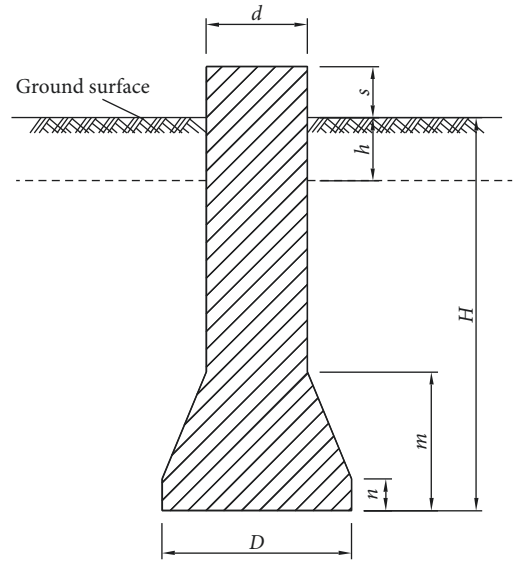

Belled pier foundation

D: diameter of bottom plate = 0.3 m

d: diameter of the column = 0.15 m

m: extended bottom height = 0.23 m

n: expand column height = 0.03 m

H: embedded depth of foundation = 0.78 m

s: exposed depth of foundation = 0.04 m

h: saline soil thickness

(b)

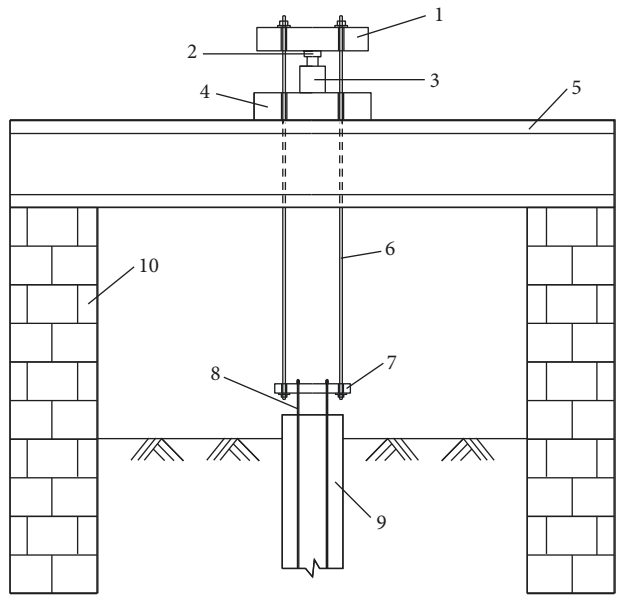

1: upper bearing plate

2: pressure sensor

3: lifting jack

4: lower bearing plate

5: steel beam

6: connecting bolts

7: connecting plate

8: connecting bolts

9: foundation

10: bearing brick column

(c)

Figure 4: Belled pier foundation in coarse-grained saline soils. (a) Vertical view of the foundation pit. (b) Cross section of the belled pier. (c) Loading system.

coarse-grained soils and were then wrapped with preservative films for 48 hours to ensure a uniform infiltration of solutions. Beneath the coarse saline soil layers, the common coarse soils were placed, compacted by the electric shocking rammer layer by layer, with each layer less than 20 cm. Soils were filled in the test pit, and each layer was compacted until the target height was reached. In addition, the uplift load was directly applied on the top of the belled pier when a 100 mm thick coarse saline soil layer in the dissolved state was filled in the foundation, i.e., the axial uplift loading test initiated. While for the other three groups before testing, the filled coarse saline soil layers with various thicknesses were firstly air-dried for about 48 hours to ensure the crystallization of the sodium sulphate solutions.

Figure 4(c) gives the uplift loading system for the belled pier foundations. According to the estimated ultimate bearing capacity of the tested foundations, the loading system includes two I-section steel beams with a length of 3.6 m, load-bearing brick columns, two lifting jacks, connecting bolts, and steel boards for bearing and connecting. The tests adopted a slow maintenance loading method and an equivalent load, not exceeding 10% of the ultimate bearing capacity. The load was applied step by step, except that the first loading level was taken to be two times the equivalent load. No impact was allowed during the loading processes and thus as the loading was maintained, the amplitude of variation is controlled to be less than ±10% of the equivalent load. The settlement of the pile top was read after the loading initiated at a time of 5, 15, 30, 45, and 60 min, and later the interval was kept to be 30 min. The standard for deformation stabilization is that the settlement of the pile top is less than 0.1 mm within an hour and appeared twice successively after either level of the load exerted for 30 min. The tests terminated when the load cannot be maintained or the settlement of the pile top at any level of the load is larger than 25 mm.

3. Results and Analysis

3.1. Failure Modes in Ground Surface. The belled pier foundation with a 100 mm-thick coarse-grained saline soil layer was taken to evaluate the surface feature of fracture during uplift, as shown in Figure 5. The high-pixel photographs in Figure 5 present the belled pier-centered surface uplifting phenomenon and circular cracks which were gradually formed. Besides, fine cracks emerged in ground surface at higher loads, and fracture rapidly expanded with penetrating cracks as the ultimate bearing capacity is approached. The overall shear failure plane was generated in this case with circular and radial-pattern fractures on ground surface. Visually, a failure cone was completely uplift off the ground.

The rectangular coordinate system was set up with the origin at the center of the belled pier and coordinate axis parallel to the brick columns. Based on the measured displacement and crack development during uplift loading, the range of uplift at each loading stage is plotted in Figure 6. Here, for the sake of simplicity, only two working conditions were considered here, i.e., Test II and Test IV. Note that the ring lines in black with the applied uplift load annotated represent the range of crack in the ground surface that stabilized at each level of loading. As the settlement of the pile top stabilized, the range of uplift for coarse-grained saline soil foundations manifested as a circumferential outward expansion with the uplift load increasing step by step. This gives the basic quantitative data for the observed circular fracture of ground surface developed with uplift loading.

Figure 7 presents the relationship between the ground uplift displacement and the distance from the foundation center at each uplift load. It shows that, at larger uplift loads, the displacement for foundations tends to grow and the range where uplift load affects enlarges, which can be regarded as a detailed presentation of how the uplift of ground develops with the applied load. Moreover, as the distance from the center increases, the uplift displacement for the monitored points is relatively smaller than those that are closer to the center, and all the four groups of tests exhibit similar variations. At the initial loading steps, the ground displacement for the points close to the center of the bell pier grows rapidly and the gradient for the displacement is relatively smooth and then it stabilizes at larger loads, while for the adjacent points, the displacement is relatively smaller.

3.2. Load-Displacement Relationship. Figure 8(a) shows the relationship between uplift load and ground displacement at the four working conditions. The curves all show a softening tendency with a peak value at a displacement of about 20 mm, which can be taken as the ultimate bearing capacity of the foundations. At a given displacement, the thicker the coarse-grained saline soils in the crystalline state, the larger the uplift load during testing, and the ultimate bearing capacity was also included. The foundation with a 100 mm-thick dissolved coarse-grained saline soil layer exhibits lowest ultimate bearing capacity. A further analysis of the measured data indicates that, in the single logarithmic coordinates, three stages can be found from the uplift load and the ratio of load to displacement, as shown in Figure 8(b).

The ultimate bearing capacity, i.e., the peak points of the curves, is plotted with the ultimate displacement, as shown in Figure 9. Clearly, the bearing capacity of the foundation significantly increased as the thickness of the crystalline soil layer increased and is larger than that in the dissolved state. Besides, the maximum displacement shows nonlinear changes, with the maximum value appearing at a thickness of 100 mm in the crystalline state, and it is two times larger for the dissolved state. This indicates that both ultimate bearing capacity and ultimate displacement are sensitive to the dissolution of coarse-grained saline soils and should be paid more attention:

(1) The first stage represents a linearly elastic relationship of ground displacement versus uplift loads. This results from the fact that, at relatively lower uplift loads, soils above the bottom board of the belled pier experienced extrusion forces and were compacted. During this stage, soils exhibit mainly the elastic compressive deformation.

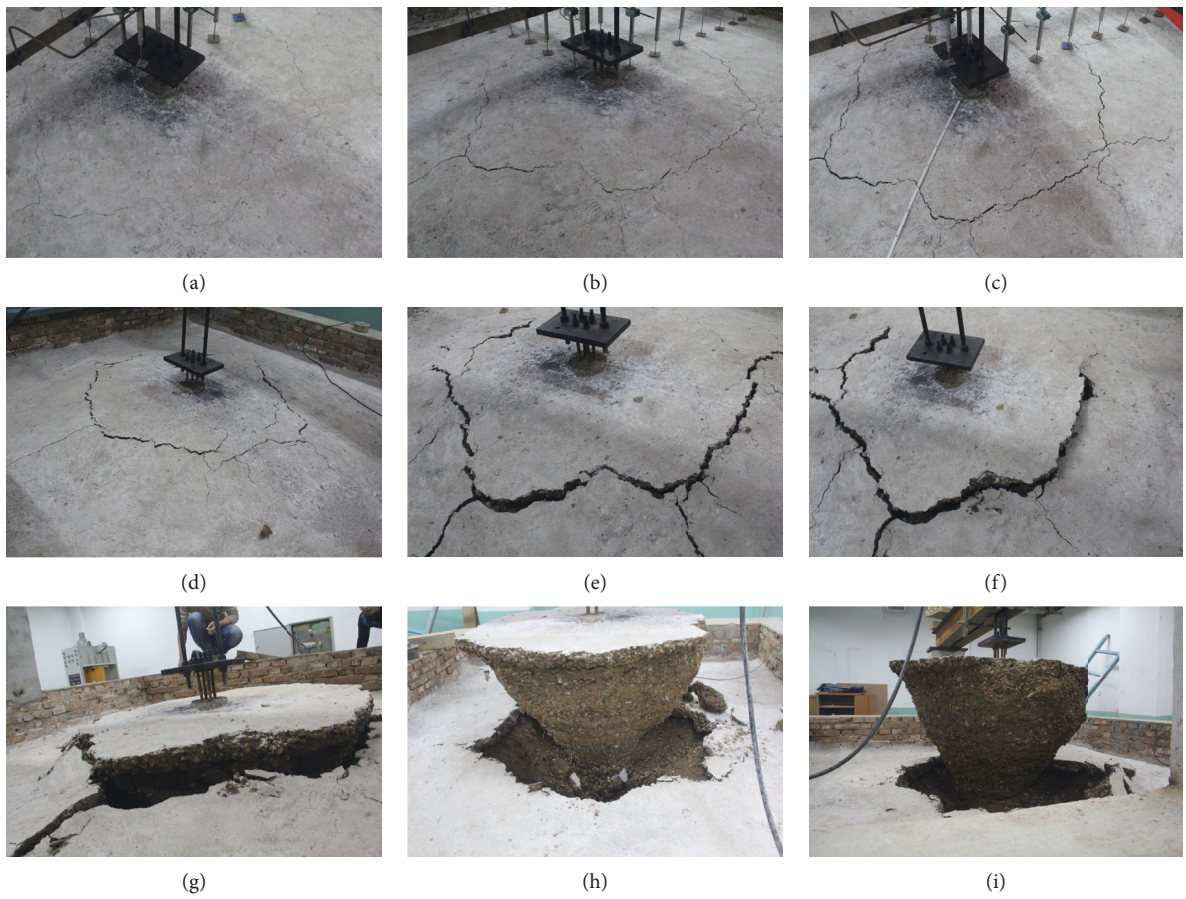

Figure 5: Failure of belled pier foundation during uplift loading. (a) t = 6.0 h. (b) t = 10.0 h. (c) t = 12.0 h. (d) t = 13.0 h. (e) t = 14.0 h. (f) t = 14.5 h. (g) t = 14.8 h. (h) t = 15.2 h. (i) t = 15.4 h.

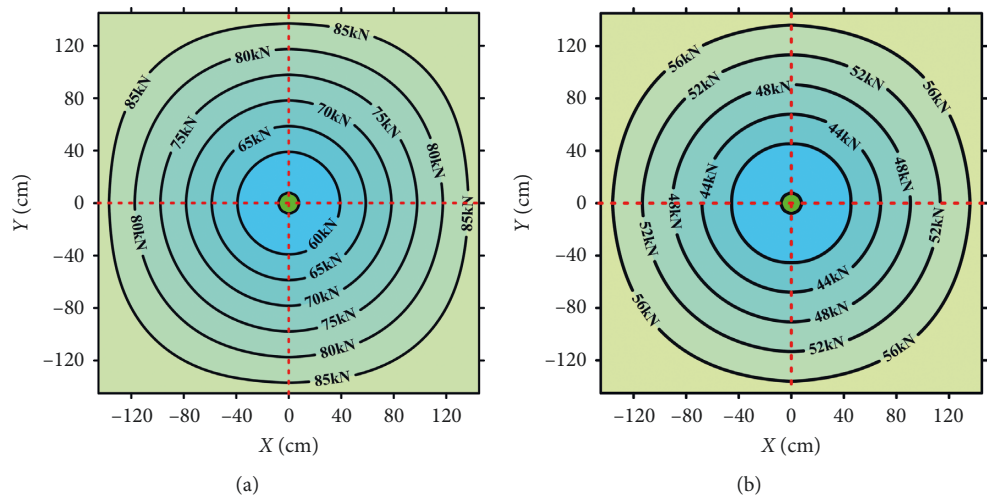

Figure 6: Range of ground uplift at various loads. (a) Test II and (b) Test IV.

(2) At higher uplift loads, the displacement of belled pier foundations tends to vary nonlinearly, and the ratio of the uplift load to the ground displacement is significantly lower than that in the first elastic stage, and the deformation of soils includes primarily the plastic deformation, rather than the elastic deformation; in this case, the plastic zone grows in soils at the stresses applied.

(3) As the ultimate bearing capacity was approached, fractures on ground surface rapidly expanded and penetrating cracks were formed in this stage, with an overall shear failure plane emerged. Soils in the

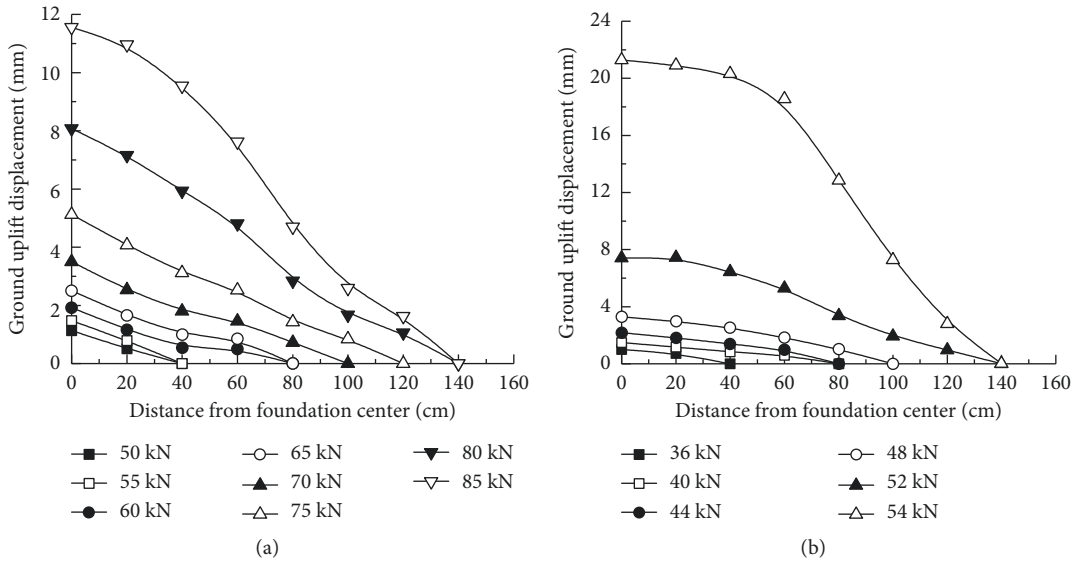

Figure 7: Ground displacement at uplift loading. (a) Test II and (b) Test IV.

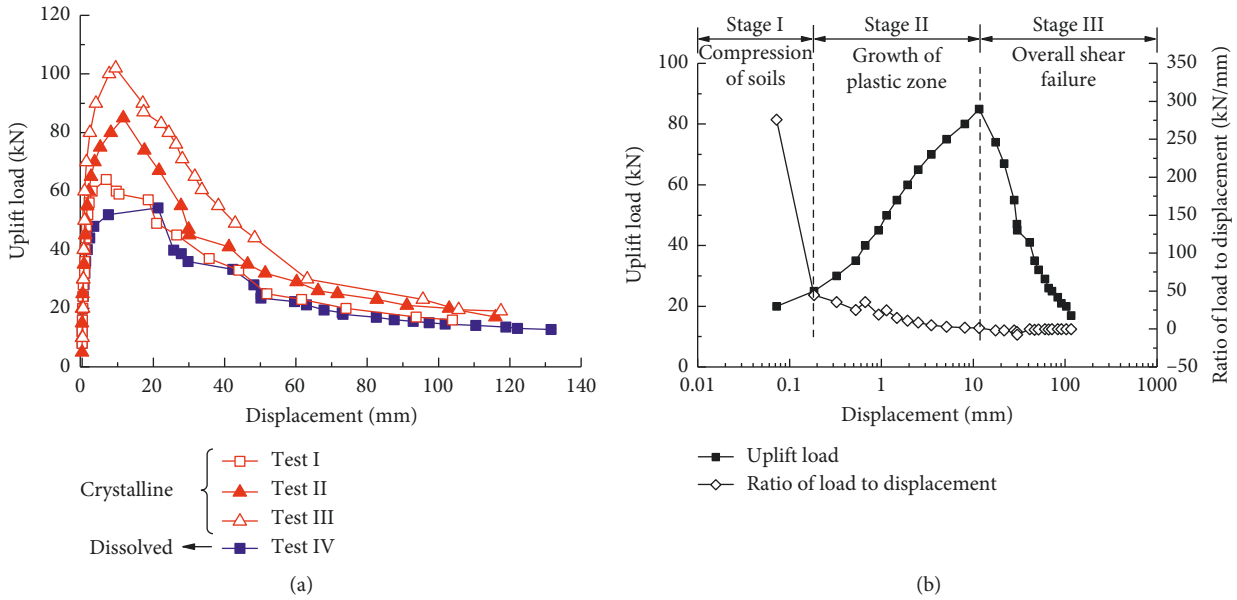

Figure 8: Uplift load-displacement curve of belled pier foundations. (a) Load-displacement relationship. (b) Ratio of load to displacement.

foundations slide along the shear failure plane and the uplift bearing capacity measured decrease considerably, identified as a load reduction that was measured by the sensors.

3.3. Failure Planes. Four typical profiles were obtained by measuring the failure cones with an interval of 45°. Figure 10 illustrates the plan view of the failure cones at the four working conditions. It shows clearly that the planar projection of the failure cones is close to circular, and the differences may result from the variance of both loading conditions and filling materials in foundations. Moreover, the planar projection for the dissolved state is larger than those in the crystalline state, proving that the range of failure that the uplift loading has caused is relatively larger, implying the fact that the ultimate bearing capacity is lower. The failure curves at each profile were measured and are plotted in Figure 11, with both ground surface and boundary line separating the two layers sketched. At four working conditions considered here, no matter what the coarse-grained soils are crystallized or dissolved, the failure modes for the belled pier foundations all show linear change from the base to the top.

Based on the morphology of the failure planes of the belled pier foundations, we can approximately use two linear relations to describe the failure curves of the two layers at each profile, respectively. The following equation was fitted by the least square method:

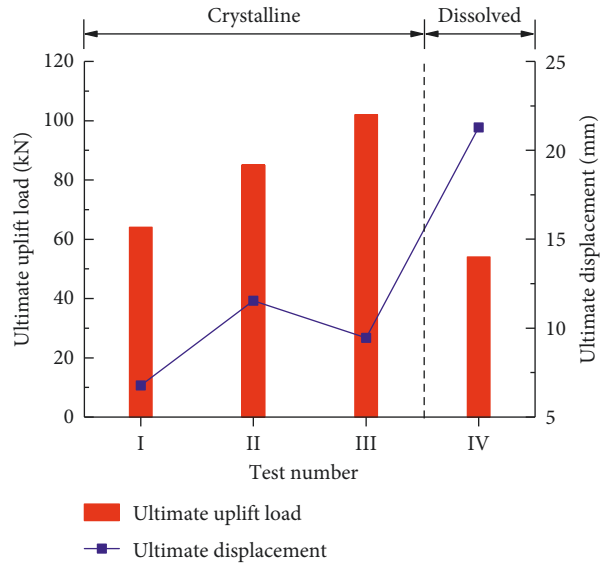

Figure 9: Comparison of both ultimate uplift bearing capacity and displacement.

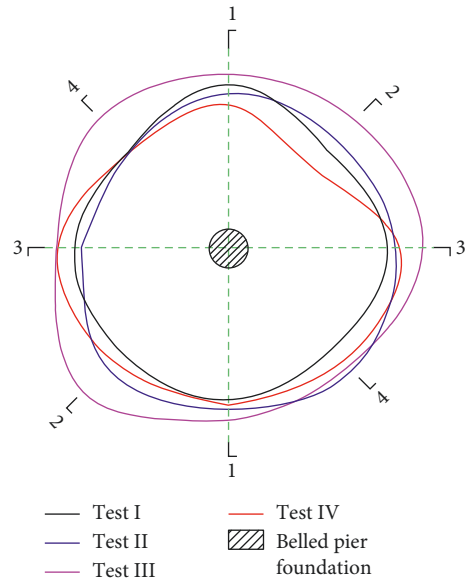

Figure 10: Planar projection of the failure cone.

$$z = m + x \cot \theta, \tag{1}$$

where x and z are the horizontal and longitudinal coordinates, respectively; m is the fitted parameter; and θ is the inclined angle of failure plane during uplifting. Taking the measured data of the third group as an example, the fitting data for failure planes are presented in Figure 12. Note that the CSS and CS represent the coarse-grained saline soils and conventional coarse soils, respectively; L and R are the directions considered in both sides of the belled pier. Both values of m and θ for each profile approach to the constants, indicating that the profile for the failure cone is approximately identical, which is supposed to happen when filling materials and loads are uniformly distributed in the belled pier foundations. Here, the measured and fitted data for the failure curves for the four working conditions were compared and presented in Figure 13. Most of points lie on or close to the line of $y = x$, which shows that the fitted curves are reasonable for describing the measured failure planes. Moreover, the fitted data for the dissolved coarse-grained saline soils exhibit larger deviation from the measured.

The statistical analysis was carried out on the angle of uplift, θ, for three kinds of strata listed in Figure 14, i.e., common coarse-grained soils and crystallized and dissolved coarse-grained saline soils. The results show that the angles of uplift at the four working conditions all show greater variance as the strata varied. If we take the mean value of the angles of uplift in the preliminary design, the

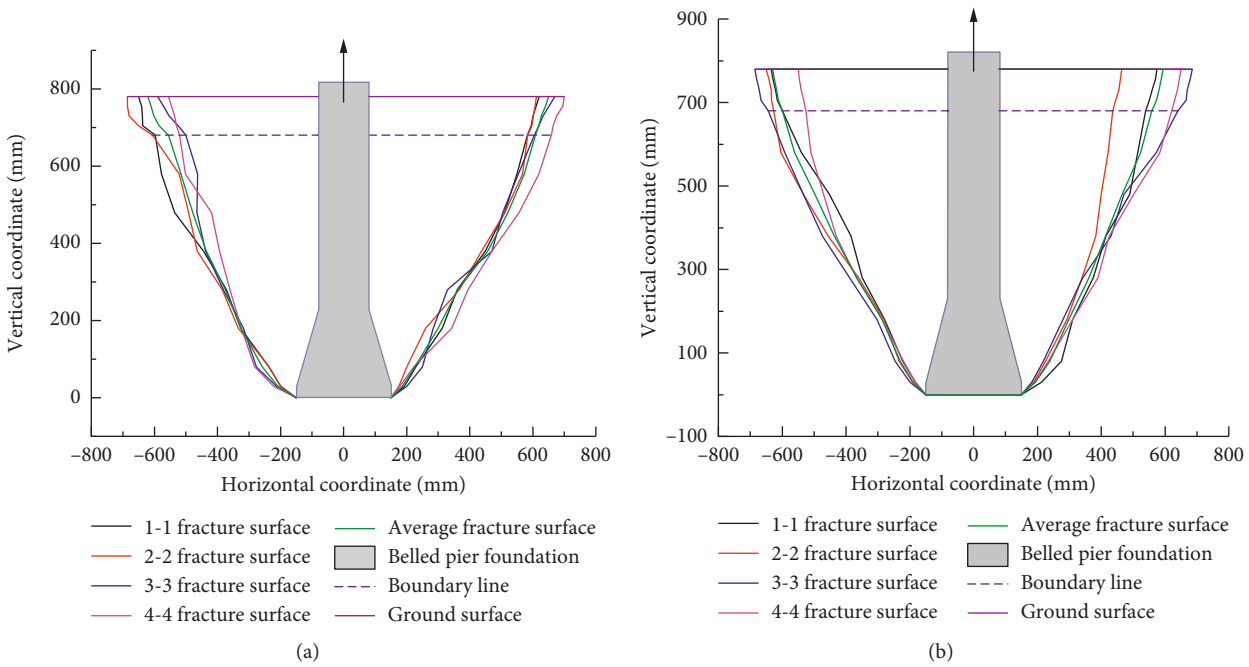

Figure 11: Ground displacement at uplift loading. (a) Test II. (b) Test IV.

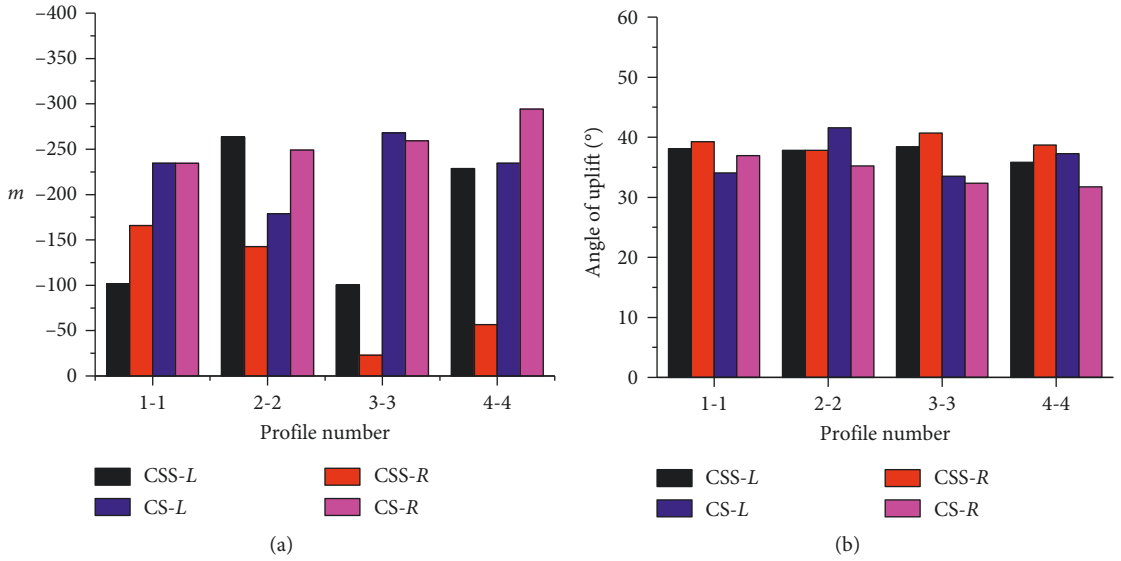

Figure 12: Fitting data for failure planes. (a) Data of m. (b) Data of θ.

angles of 32°, 34°, and 18°, corresponding to the above three strata, and can be used for engineers' reference for the sake of safety. Thus, the simplified failure modes at the four working conditions can also be adopted in engineering design. Note that the precipitation or evaporation of the ground should be carefully considered in engineering design. For example, the angle of uplift for coarse-grained saline soils shows little difference from that for common coarse-grained soils in the dry season, while the salinity in soils can be dissolved as the precipitation occurs, and in this case, the angle of uplift decreases significantly. Note that the ultimate uplift bearing capacity mainly includes three components such as the bearing capacity of the ground shear failure plane and the self-weight of both foundation and uplift fracture cone. The first two components will be significantly reduced at smaller uplift angles, further leading to the decrease in the ultimate uplift bearing capacity.

4. Modelling of Uplift Behaviour Incorporating a Practical Interface Model

4.1. Constitutive Equations. Reinforced concrete (RC) was utilized in producing the belled piers, and its deformation can be simplified as linearly elastic in that the failure of belled

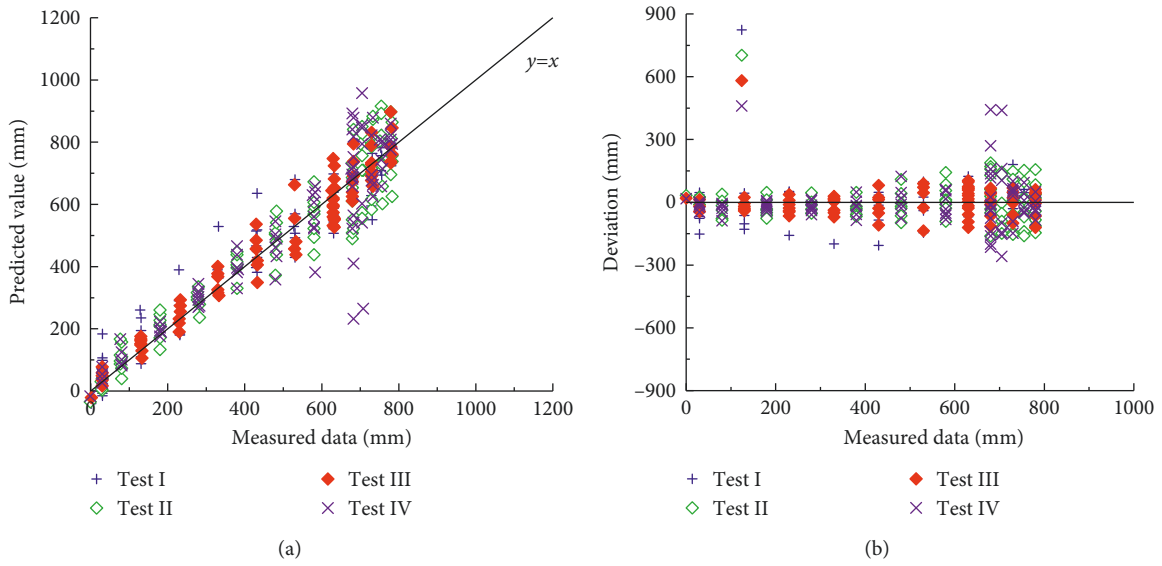

Figure 13: Comparison of predicted and measured curves. (a) Predicted and measured data. (b) Deviation.

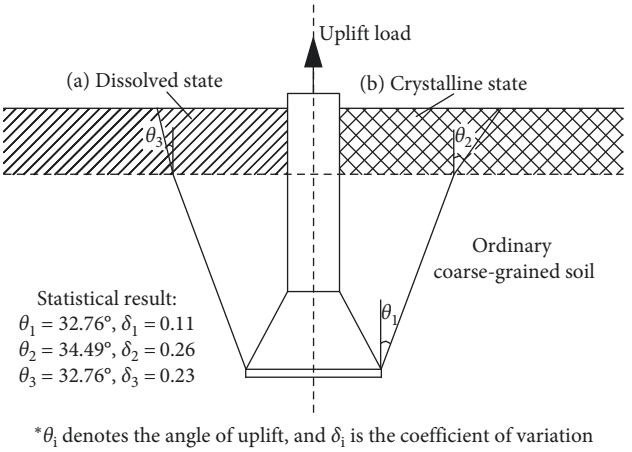

Figure 14: Failure modes for belled pier foundation in coarse-grained saline soils.

pier foundations in most cases originates from the failure of foundation. Thus, the yield and even failure are not assumed to occur for belled piers. The elastic constitutive equation for RC can be given as

$$\sigma_{ij} = 2G\varepsilon_{ij} + \frac{3E\mu}{(1+\mu)(1-2\mu)}\varepsilon_{\mathrm{m}}\delta_{ij}, \tag{2}$$

where σ_{ij} and ε_{ij} are the stress and strain tensors; E and μ are the elastic modulus and Poisson's ratio; ε_{m} is the mean strain; and δ_{ij} is the unit matrix.

The belled pier foundations are in general embedded in shallow layers, and the stress-strain relationship for soils in that case can be simply described by an ideally elastoplastic constitutive equation. As the soils in foundations deform within the elastic limit, the above Equation (2) is obeyed, while the components of stress and strain tensors are calculated by the following equation of plasticity when the ideally plastic state is reached:

$$\begin{cases} de_{ij} = \dfrac{1}{2G}ds_{ij} + d\lambda s_{ij}, \\ d\sigma_{\mathrm{m}} = 3Kd\varepsilon_{\mathrm{m}}, \end{cases} \tag{3}$$

where e_{ij} and s_{ij} are the deviatoric strain and stress tensors, respectively; σ_{m} is the mean stress tensor; and K is the volumetric elastic modulus. The parameter $d\lambda$ can be calculated by

$$d\lambda = \frac{3}{2}\frac{s_{ij}de_{ij}}{\sigma_{\mathrm{s}}^2}, \tag{4}$$

where σ_{s} is the yield limit. The Mohr–Coulomb yield criterion was adopted here to simulate the possible compressive shearing and tensile damage of pile soils during uplifting, as presented in Figure 15.

The interface between belled piers and soils around was modelled by interface with zero thickness and can be

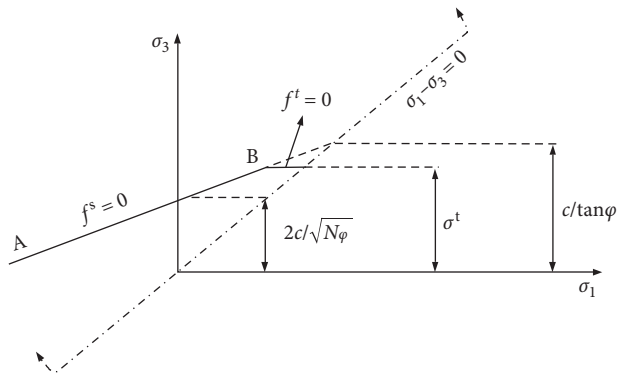

Figure 15: The Mohr–Coulomb yield criterion in principal stress space.

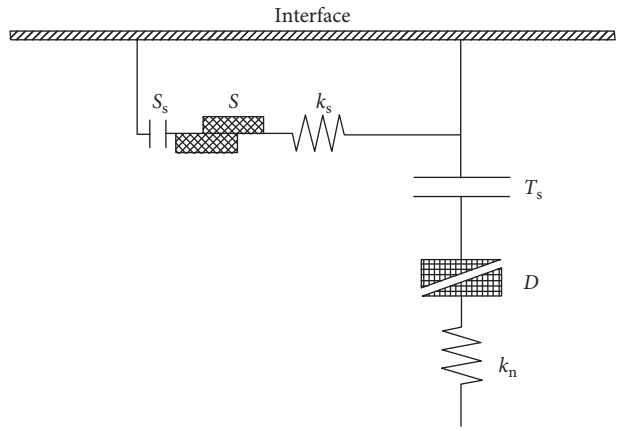

S: slider
T_s: tensile strength
S_s: shear strength
D: dilation angle
k_s: shear stiffness
k_n: normal stiffness

Figure 16: Schematic diagram of the practical interface model.

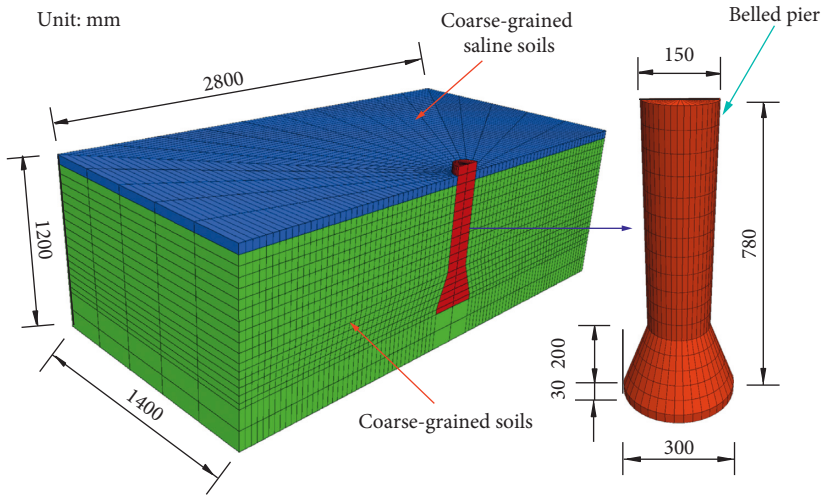

Figure 17: Geometric model in computation.

Table 1: Model parameters in computation.

Parameters	Belled pier	Crystalline CSS	Dissolved CSS	CS	Interface crystalline	Interface dissolved	Interface with CS
E (MPa)	30000	1300	200	600	—	—	—
μ	0.2	0.25	0.30	0.30	—	—	—
r (kN/m^3)	25	22.6	23.0	21.5	—	—	—
c (MPa)	1.2	0.048	0.03	0.042	0.2	0.008	0.008
ϕ (°)	50	44	27	35	25	25	25
k_n (MPa)	—	—	—	—	0.21	0.15	0.15
k_s (MPa)	—	—	—	—	0.01	0.007	0.007

generalized in Figure 16, with the normal and tangential stresses determined by

$$\begin{cases} F_n = k_n u_n A, \\ F_s = k_s u_s A, \end{cases} \tag{5}$$

where the subscripts n and s represent the normal and tangential directions; F and u are the force and displacement of the interface; k is the stiffness; and A is the area.

The maximum shear stress in the interface was calculated by the Mohr–Coulomb yield limit:

$$F_{smax} = cA + F_n \tan \phi, \tag{6}$$

where c and ϕ are the cohesion and internal friction angle of the interface, respectively.

The following should be satisfied if $F_s > F_{smax}$:

$$\sigma_{nmax} = \sigma_n + \frac{|F_s| - F_{smax}}{Ak_s} \tan \psi k_n, \tag{7}$$

where F_{smax} is the maximum tangential stress of the interface; σ_n is the normal stress; and ψ is the dilatancy angle. Provided that the tensile failure occurs at both sides of the interface, then F_n and F_s are assumed to be zero.

4.2. Geometric Model and Parameters. The geometric model based on the borehole data is presented in Figure 17, including three main components such as the reinforced concrete belled pier, coarse-grained saline soils, and conventional coarse soils. The thickness for the second was controlled to be 50, 100, and 150 mm, while 100 mm for the dissolved state. The normal displacement was restrained in four sides and the bottom, while the upper is assumed displacement free, with a normal uplift load applied on the top of the belled pier, considered as the z direction. The parameters in computation are listed in Table 1.

4.3. Comparison of Measured and Calculated Results. Figure 18 illustrates the simulated load-displacement curves at four working conditions. The curves all exhibit similar changes that the ratio of load to displacement declines and is hardening. The simulated and measured data were plotted in Figure 19, and comparisons prove that the simulated results agree well with the measured data. Most of the data points corresponding to the lower uplift loads are all close to the $y = x$ straight line, while for those at higher loads, larger deviations between the two sets of data

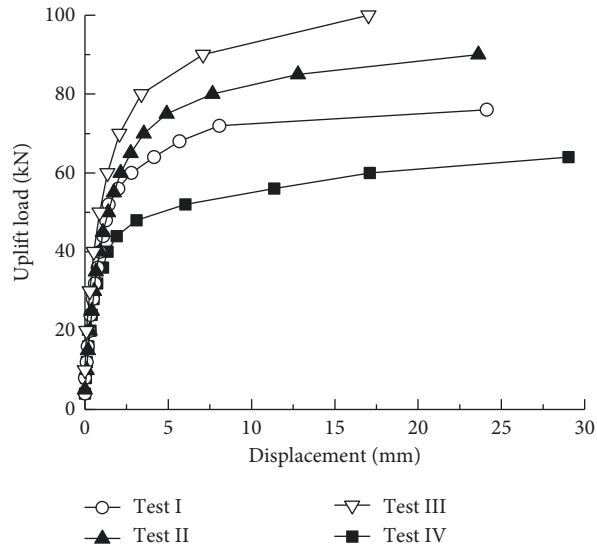

Figure 18: Load-displacement curves of belled pier foundations.

can be observed. The heterogeneity of filled materials may account for this discreteness that cannot be well modelled by an ideally elastoplastic constitutive equation. The uplift load characterized by an abrupt change in the load-displacement curves was taken as the ultimate bearing capacity. The simulated data are plotted in Figure 20 together with the measured. It shows that the two sets of data coincide well, and the ultimate bearing capacity for the foundation in the crystalline state is higher than that in the dissolved state. However, similar changes can be noted as the depth of coarse-grained saline soils increases, proving that the simulation gives a reliable result for the working conditions considered here.

The failure planes of the belled pier foundation during uplifting can be determined by the growth of the plastic zone until a critical limit surface is reached, identified by a visually observed penetrating range. Figure 21 gives the failure modes of soil mass at the four working conditions. Axisymmetric failure envelops centered on the belled pier were found from the bottom upward. The angle of uplift for foundations with CS is higher than that with dissolved CSS, while it is lower than that in crystalline state, which shows good agreement with the measured data. The failure planes calculated and measured are both plotted in Figure 22. These two profiles exhibit similar pattern, with a small discrepancy between the two, and this may be

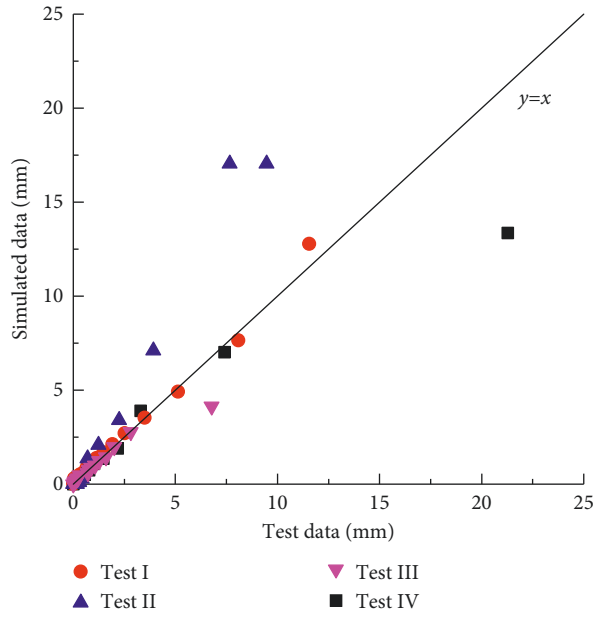

Figure 19: Comparison of measured and simulated results.

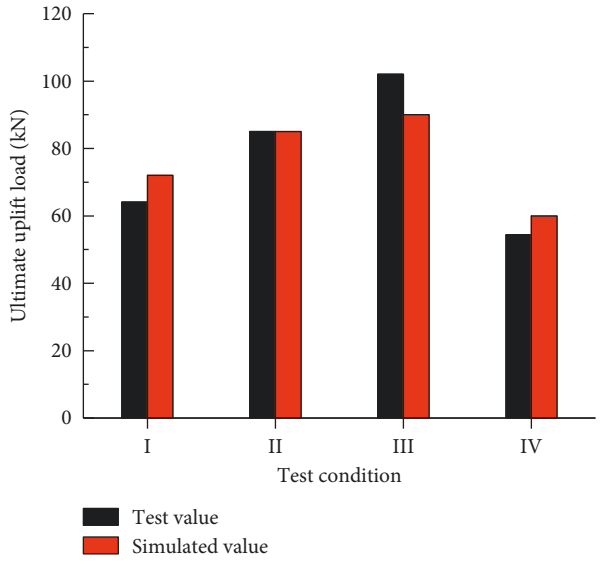

Figure 20: Comparison of measured and simulated uplift bearing capacity.

caused by the simplification of the stratum feature in computation.

Figure 23 illustrates the development of plastic range for the belled pier foundation with a coarse-grained saline soil layer with a thickness of 100 mm. It clearly shows that the plastic zone firstly emerged from the bottom of the belled pier, implying that the uplift load has been transferred from the top to the bottom and eventually exerted on surrounding soils. The plastic zone enlarged from the bottom upward with the increase in the loading level, and finally the penetrating plastic zone was produced. Also, at the final stage of uplift loading, the range of the plastic zone at specified depths mainly develops horizontally, indicating that the load transferred by the friction between pile and soil is limited. Visually, the pattern of the plastic zone is quite close to the failure plane obtained based on the displacement isolines.

5. Conclusions

The result of this result of model tests on belled pier foundations with coarse-grained saline soils of different thicknesses and two occurrence modes has been provided. Modelling of uplift behaviour of belled pier foundations was also carried out based on a practical interface. The main conclusions are as follows:

(1) Considerable ground uplift phenomena were observed during model tests and the belled

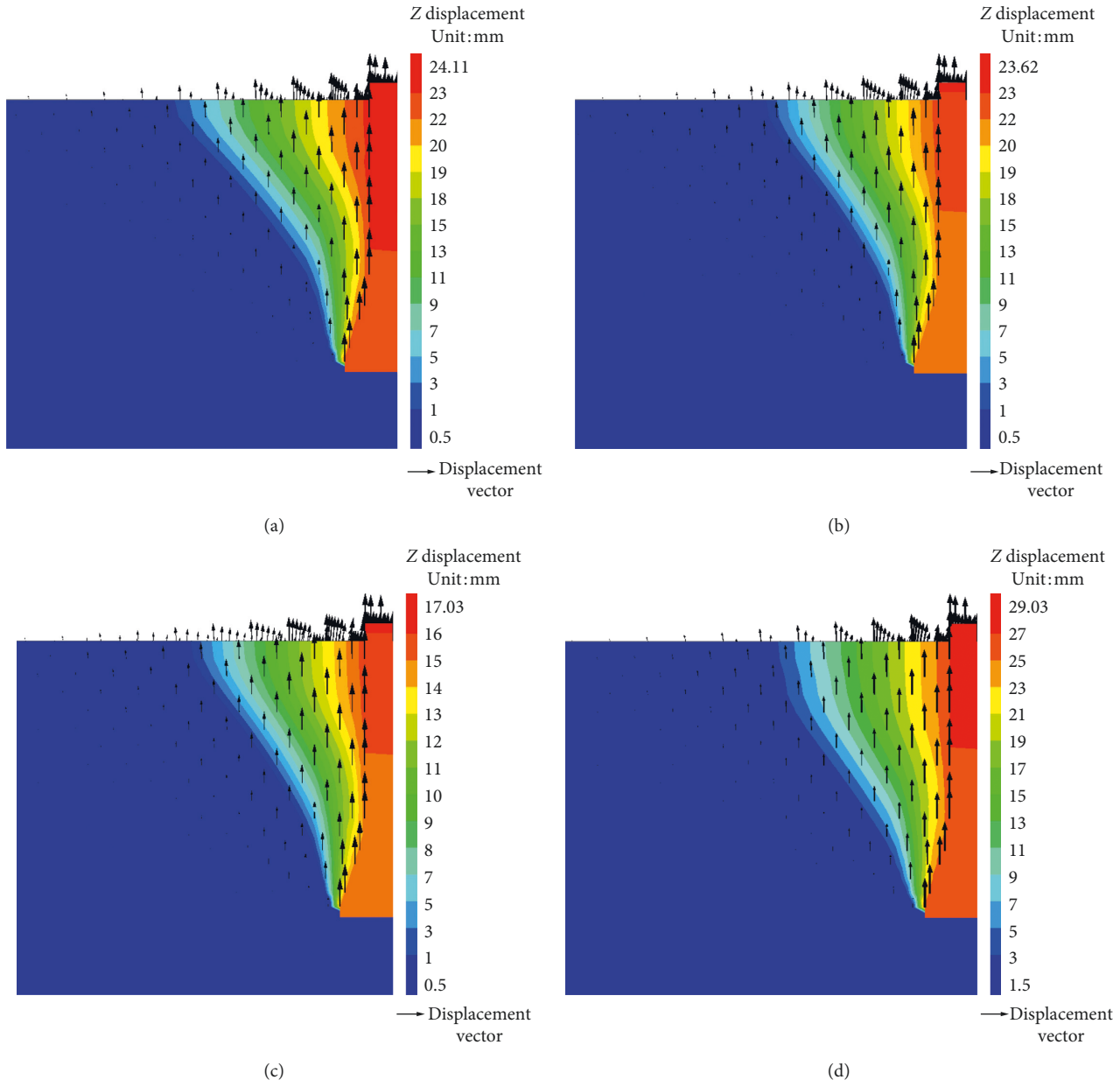

Figure 21: The calculated failure plane. (a) Test I. (b) Test II. (c) Test III. (d) Test IV.

pier-centered circular cracks emerged, manifesting as that, at larger uplift loads, the cracks tend to enlarge, rapidly extend, and penetrate the ground surface, where the circular and radial-pattern fractures were noted. An overall shear failure plane appeared eventually.

(2) The relationship between uplift load and displacement shows softening characteristics, and when the ultimate bearing capacity is reached, a stage of load reduction was observed. As the thickness of coarse saline soil layer increased, the bearing capacity increased significantly while lowered for foundations in the dissolved state.

(3) The failure planes for foundations in both crystalline and dissolved states can be simplified as a linear form. Based on the measured data of each profile at the four working conditions, the angles of uplift for the three kinds of stratums are 32°, 34°, and 18°, respectively, and can be used for design.

(4) Comparison of calculated and measured failure planes proves a good coincidence, and axisymmetric failure envelops centered on the belled pier were noted. The angle of uplift for foundations with CS is higher than that with dissolved CSS, while it is lower than that in the crystalline state. Besides, the plastic zone enlarged from the bottom upward with the

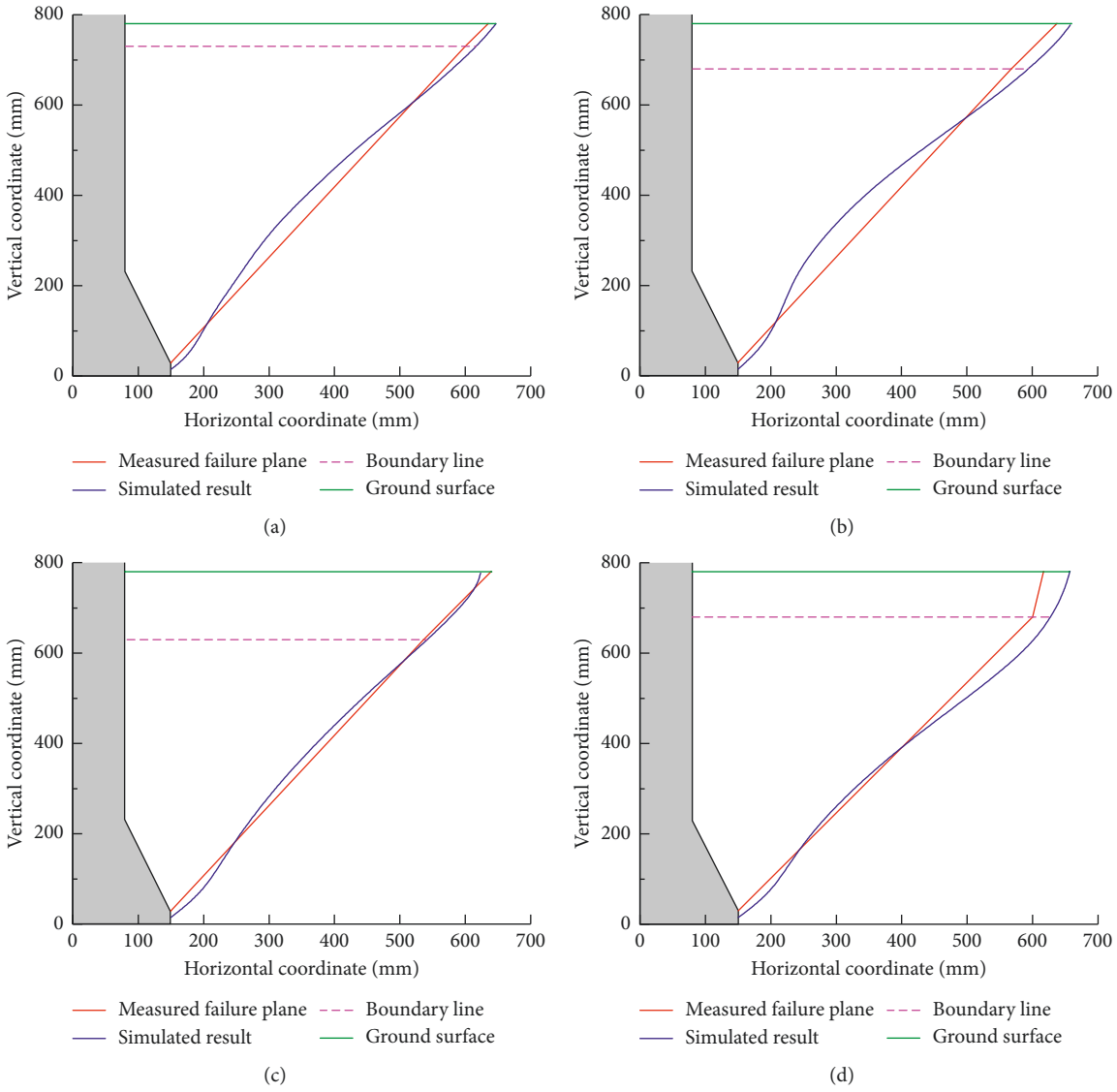

Figure 22: Comparison of calculated and measured failure plane. (a) Test I. (b) Test II. (c) Test III. (d) Test IV.

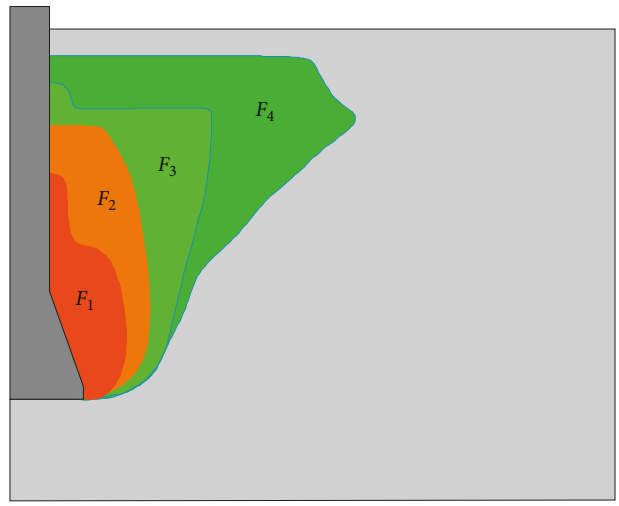

Load procedure:
F_1 = 30 kN
F_2 = 50 kN
F_3 = 70 kN
F_4 = 85 kN

Figure 23: Plastic zone development of the belled pier foundation.

increase in the loading level, and finally, the penetrating plastic zone was produced.

Data Availability

The data used to support the findings of this study are available from the corresponding author upon request.

Disclosure

Northwest Electric Power Design Institute Co., Ltd., of China Power Engineering Consulting Group had final approval of the manuscript.

Conflicts of Interest

The authors declare that there are no conflicts of interest regarding the publication of this paper.

Acknowledgments

This research was financially supported by the National Natural Science Foundation of China (Nos. 51478385, 51778528, 51208409, and 51408486). These supports are greatly appreciated.

References

[1] Y. M. Lai, M. K. Liao, and K. Hu, "A constitutive model of frozen saline sandy soil based on energy dissipation theory," *International Journal of Plasticity*, vol. 78, pp. 84–113, 2016.

[2] M. K. Liao, Y. M. Lai, and C. Wang, "A strength criterion for frozen sodium sulfate saline soil," *Canadian Geotechnical Journal*, vol. 53, no. 7, pp. 1176–1185, 2016.

[3] A. Yakirevich, P. Berliner, and S. Sorek, "A model for numerical simulating of evaporation from bare saline soil," *Water Resources Research*, vol. 33, no. 5, pp. 1021–1033, 1997.

[4] C. Zhang, L. Li, and D. Lockington, "Numerical study of evaporation-induced salt accumulation and precipitation in bare saline soils: mechanism and feedback," *Water Resources Research*, vol. 50, no. 10, pp. 8084–8106, 2014.

[5] L. U. Arenson and D. C. Sego, "The effect of salinity on the freezing of coarse-grained sands," *Canadian Geotechnical Journal*, vol. 43, no. 3, pp. 325–337, 2006.

[6] X. L. Lu, W. F. Zheng, Y. F. Cheng, and R. M. Tong, "Experimental study on excavated foundation of transmission line gravelly soils in gobi area of northwest China," *Chinese Journal of Geotechnical Engineering*, vol. 31, no. 11, pp. 1779–1783, 2009, in Chinese.

[7] G. Imancli, M. R. Kahyaoglu, G. Ozden, and A. S. Kayalar, "Performance functions for laterally loaded single concrete piles in homogeneous clays," *Structural Engineering and Mechanics*, vol. 33, no. 4, pp. 529–537, 2009.

[8] J. J. Kumara, T. Kurashina, and Y. Kikuchi, "Effects of pile geometry on bearing capacity of open-ended piles driven into sands," *Geomechanics and Engineering*, vol. 11, no. 3, pp. 385–400, 2016.

[9] A. Mohebkhah, "Bearing capacity of strip footings on a stone masonry trench in clay," *Geomechanics and Engineering*, vol. 13, no. 2, pp. 255–267, 2017.

[10] V. N. Khatri, S. P. Debbarma, R. K. Dutta, and B. Mohanty, "Pressure-settlement behavior of square and rectangular skirted footings resting on sand," *Geomechanics and Engineering*, vol. 12, no. 4, pp. 689–705, 2017.

[11] D. Chae, W. Cho, and H. Y. Na, "Uplift capacity of belled pile in weathered sandstone," *International Journal of Offshore and Polar Engineering*, vol. 22, no. 4, pp. 297–305, 2012.

[12] Z. Z. Qian, X. L. Lu, X. Han, and R. M. Tong, "Interpretation of uplift load tests on belled piers in Gobi gravel," *Canadian Geotechncial Journal*, vol. 52, no. 7, pp. 992–997, 2015.

[13] K. Ikeda, Y. Yamakawa, K. Morita, S. Horimoto, and T. Ozaki, "Study on applicability of elasto-plastic finite element analysis to the estimation of uplift behavior of belled pier," *Doboku Gakkai Ronbunshuu C*, vol. 63, no. 1, pp. 1–12, 2007, in Japanese.

[14] S. B. Gurung, Y. Nakazima, S. Sakajo, and O. Kusakabe, "Centrifugal modeling of enlarged base foundation subjected to pull-out force," *Soils and Foundations*, vol. 38, no. 4, pp. 105–113, 1998.

[15] Z. Wen, Q. H. Yu, M. L. Zhang, K. Xue, L. Z. Chen, and D. S. Li, "Stress and deformation characteristics of transmission tower foundations in permafrost regions along the Qinghai-Tibet power transmission line," *Cold Regions Science and Technology*, vol. 121, pp. 214–225, 2015.

[16] C. V. Stas and F. H. Kulhawy, *Critical Evaluation of Design Methods for Foundations under Axial Uplift and Compression Loading*, Electric Power Research Institute USA, Palo Alto, CA, USA, 1984.

[17] L. Sheng, L. Ma, P. Jiang, F. Huang, and H. Wu, "Digital soil mapping to enable classification of the salt-affected soils in desert agro-ecological zones," *Agricultural Water Management*, vol. 97, no. 12, pp. 1944–1951, 2010.

[18] R. Wang, S. Wan, Y. Kang, and C. Dou, "Assessment of secondary soil salinity prevention and economic benefit under different drip line placement and irrigation regime in northwest China," *Agricultural Water Management*, vol. 131, no. 1, pp. 41–49, 2014.